Electronic Supplementary Information

Surface Nitrogen-modified 2D Titanium Carbide (MXene) with High Energy Density for Aqueous Supercapacitor Applications

Yapeng Tian[a], Wenxiu Que[*,a], Yangyang Luo[a], Chenhui Yang[a], Xingtian Yin[a],
Ling Bing Kong[*, b]

[a] Electronic Materials Research Laboratory, International Center for Dielectric Research, Key Laboratory of the Ministry of Education, Shaanxi Engineering Research Center of Advanced Energy Materials and Devices, School of Electronic & Information Engineering, Xi'an Jiaotong University, Xi'an 710049, Shaanxi, People's Republic of China

[b] College of New Materials and New Energies, Shenzhen Technology University, Shenzhen 518118, Guangdong, People's Republic of China

[*] *Corresponding author*: Prof. W. Que, Tel. & Fax: +86-29-83395679.

E-mail address: wxque@mail.xjtu.edu.cn (W. Que), konglingbing@sztu.edu.cn (L.B. Kong)

Lists of Content

1 A g^{-1} to 10 A g^{-1}. (c) Specific capacitance of the N-$Ti_3C_2T_x$-200 electrode at different scan rates. (d) Nyquist plot of the N-$Ti_3C_2T_x$-200 electrode from 100 kHz to 10 mHz. The inset is a magnification in the high-frequency region.

Fig. S10 The fitted curves for the $Ti_3C_2T_x$, N-$Ti_3C_2T_x$, N-$Ti_3C_2T_x$-200, N-$Ti_3C_2T_x$-300 and N-$Ti_3C_2T_x$-500 samples.

Fig. S11 (a-b) TEM images of the $Ti_3C_2T_x$ nanosheets, (c) Cross section SEM images of the N-$Ti_3C_2T_x$-300 films, (d-h) SEM images of the N-$Ti_3C_2T_x$-300 films, (e, f, g and h) EDS elemental mappings of Ti, F, N and C.

Fig. S12 (a) XPS survey spectrum of the N-$Ti_3C_2T_x$-300 films. (b) High-resolution XPS spectra of the deconvoluted N 1s peaks of the N-$Ti_3C_2T_x$-300 films. (c) High-resolution XPS spectra of the deconvoluted O1s peaks of the N-$Ti_3C_2T_x$-300 films.

Fig. S13 F 1s XPS spectra of the $Ti_3C_2T_x$, N-$Ti_3C_2T_x$, and N-$Ti_3C_2T_x$-300 samples.

Fig. S14 The XRD spectra of the $Ti_3C_2T_x$, $Ti_3C_2T_x$-300 and N-$Ti_3C_2T_x$-300 films and the magnified patterns over 5-12°.

Fig. S15 (a) CV curves of the $Ti_3C_2T_x$ film electrode at scan rates from 2 mV s^{-1} to 200 mV s^{-1}, in 3 M H_2SO_4. (b) GCD curves of the $Ti_3C_2T_x$ film electrode at current densities from 1 A g^{-1} to 200 A g^{-1}. (c) Nyquist plots of the three electrodes at frequencies from 100 kHz to 10 mHz. The inset is the zoom-in profile of the high-frequency region.

Fig. S16 Electrochemical properties tested in the three-electrode configuration with Swagelok. (a) CV curves of the $Ti_3C_2T_x$-300 film electrode at scan rates from 2 mV s^{-1} to 200 mV s^{-1}. (b) Gravimetric capacitances of the $Ti_3C_2T_x$, $Ti_3C_2T_x$-300and N-$Ti_3C_2T_x$-300 electrodes at different scan rates.

Fig. S17 SEM images of the cross section for the N-$Ti_3C_2T_x$-300 film electrode after 18000 cyclings at different magnification (a-c). (d) SEM images of the N-$Ti_3C_2T_x$-300 sample after after 18000 cyclings and the corresponding EDS elemental mappings of C, N, Ti and F.

Fig. S18 CV partition analysis showing capacitive contribution to total current density at 10 mV s^{-1} for the accordion-like $Ti_3C_2T_x$ film electrode.

Fig. S19 CV curves of the $Ti_3C_2T_x$ film based symmetric supercapacitors at scan rates from 2 mV s^{-1} to 500 mV s^{-1} in 3 M H_2SO_4.

Synthesis of Ti_3AlC_2 powders.

Ti_3AlC_2 powders were prepared by using atmosphere sintering method, with mixed powders of TiC (2-4 μm, 99% purity, Aladdin), Al (1-3 μm, 99.5% purity, Aladdin) and Ti (≤ 48 μm, 99.99% purity, Aladdin) at a molar ratio of 2:1.2:1. The mixed powders were ball-milled in absolute ethyl alcohol for 4 h at a speed of 350 rpm. Then, the mixture was sintered at 1400 °C for 2 h in Ar in a tube furnace. The sintered product was further grinded with a mortar to obtain powders, which were then sieved through a 400 mesh screen.

Preparation of $Ti_3C_2T_x$-300 film sample.

The $Ti_3C_2T_x$-300 film sample was prepared by putting the $Ti_3C_2T_x$ film treated at 300 °C under Ar atmosphere for 1 h.

Preparation of d-N-$Ti_3C_2T_x$.

The d-N-$Ti_3C_2T_x$ samples were prepared by putting 1 g N-$Ti_3C_2T_x$ into 100 mL deoxygenated water in a glass bottle, followed by stirring for 1 h. Then, the mixture was sonicated for 5 h and centrifuged for 1 h at 2000 rpm. Finally, the powders, named as d-N-$Ti_3C_2T_x$, were collected through vacuum filtration.

Preparation of the N-$Ti_3C_2T_x$-200, N-$Ti_3C_2T_x$-300, and N-$Ti_3C_2T_x$-500 electrodes.

The working electrodes were fabricated by mixing active materials (N-$Ti_3C_2T_x$-200 powders, N-$Ti_3C_2T_x$-300 powders, and N-$Ti_3C_2T_x$-500 powders), acetylene black and binder (PVDF) at a weight ratio of 85:10:5. Then, the mixture suspension was dropped onto a piece of nickel foam (1×2 cm^2), followed by drying in a vacuum oven at 120 ºC for 12 h. After that, the obtained nickel foam was pressed under 10 MPa for 1 min. Finally, the as-prepared working electrodes were dried in a vacuum oven at 80 ºC for 12 h. Mass loading of active material in each current collector was about 1.8 mg cm^{-2}.

Electrochemical performance measurements of the $Ti_3C_2T_x$, N-$Ti_3C_2T_x$-300, and N-$Ti_3C_2T_x$-500 electrodes.

To test the N-$Ti_3C_2T_x$-200, N-$Ti_3C_2T_x$-300, and N-$Ti_3C_2T_x$-500 electrodes, Pt sheet (1×1 cm^2) and saturated calomel electrodes (SCE) were used as the counter electrode and the reference electrode, respectively, with 1 M Li_2SO_4 solution as the electrolyte. Cyclic voltammograms (CVs) were obtained over the voltage range between -0.9 V and -0.3 V at scan rates of 2-200 mV s^{-1}. Galvanostatic charge-discharge (GCD) measurements were carried out at current densities of 1-10 A g^{-1}, over a voltage range between -0.9 V and -0.3 V. Electrochemical impedance spectroscopy (EIS) was performed at an

open circuit potential of 5 mV and frequencies ranging from 10 mHz to 100 kHz.

Calculation.

Gravimetric capacitance, C_g (F g^{-1}), of the working electrode can be calculated from the CV curve by using the following equation (S1):

$$C_g = \int I \, dV / (m \, s \, \Delta V), \quad \text{(S1)}$$

where I (A) is the response current of the CV curve, s (V s^{-1}) is the scan rate, ΔV (V) is the potential window and m (g) is the mass loaded in working electrode.

Volumetric capacitance C_v (F cm^{-3}) of the working electrode can be also calculated from the CV curve by using the following equation (S2):

$$C_v = \int I \, dV / (V \, s \, \Delta V), \quad \text{(S2)}$$

where V (cm^{-3}) is the volume of the film in working electrode.

Gravimetric capacitance $C_{g,cell}$ (F g^{-1}) of the symmetric supercapacitor can be calculated from the CV curve by using the following equation (S3):

$$C_{g,cell} = \int I \, dV / (m \, s \, \Delta V), \quad \text{(S3)}$$

where I (A) is the response current of the CV curve, s (V s^{-1}) is the scan rate, ΔV (V) is the potential window and m (g) is the total mass loaded in two electrodes.

Volumetric capacitance $C_{v,cell}$ (F g^{-1}) of the symmetric supercapacitor can be calculated from the CV curve by using the following equation (S4):

$$C_{v,cell} = \int I \, dV / (V \, s \, \Delta V), \quad \text{(S4)}$$

where V (cm^{-3}) is the total volume of the film in two electrodes.

Energy density (E) and power density (P) of the symmetric supercapacitor can be calculated according to the following equations:

$$E_g = 1/2 \; C_{g,cell} \, \Delta V^2 \quad \text{(S5)}$$

$$E_v = 1/2 \; C_{v,cell} \, \Delta V^2 \quad \text{(S6)}$$

$$P = 3600 \; E/\Delta t, \quad \text{(S7)}$$

where ΔV is the voltage range of one sweep segment and Δt is the time for a sweep segment.

Table S1 XPS results of the samples.

Samples	Ti 2p (at.%)	C 1s (at.%)	O 1s (at.%)	N 1s (at.%)	F1s (at.%)
$Ti_3C_2T_x$	16.76	55.97	11.80	0.89	14.58
N-$Ti_3C_2T_x$	15.52	31.30	11.88	7.99	33.32
N-$Ti_3C_2T_x$-300	16.30	41.97	17.82	4.62	19.29
N-$Ti_3C_2T_x$-500	18.57	42.51	18.95	1.26	18.71
$Ti_3C_2T_x$ film	25.19	50.28	13.98	1.12	9.44
N-$Ti_3C_2T_x$-300 film	23.77	49.49	15.81	3.10	7.82

Table S2 Fitting parameters from the EIS.

Fitting parameters	Rs (Ω cm^2)	Rct (Ω cm^2)	CPE (S Sec^n/cm^2)	Zw (S $Sec^{1/2}$)	Cd (uF)
$Ti_3C_2T_x$	4.325	0.6766	0.0002312	0.08774	22.7
N-$Ti_3C_2T_x$	3.32	0.8904	0.0005604	0.1346	44.7
N-$Ti_3C_2T_x$-200	3.103	1.008	0.0002265	0.0536	26.1
N-$Ti_3C_2T_x$-300	2.788	1.816	0.001421	0.1224	39.3
N-$Ti_3C_2T_x$-500	3.359	0.5628	0.0004462	0.1367	29.28

Fig. S1

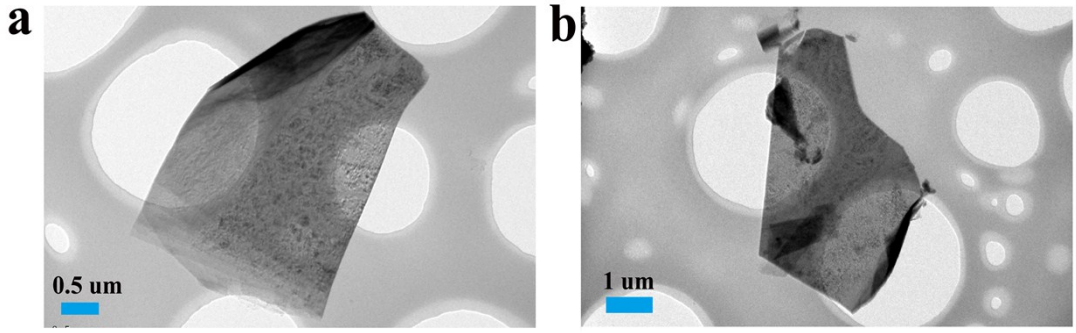

Fig. S1 TEM images of the d-N-$Ti_3C_2T_x$ sample (a, b)

Fig. S2

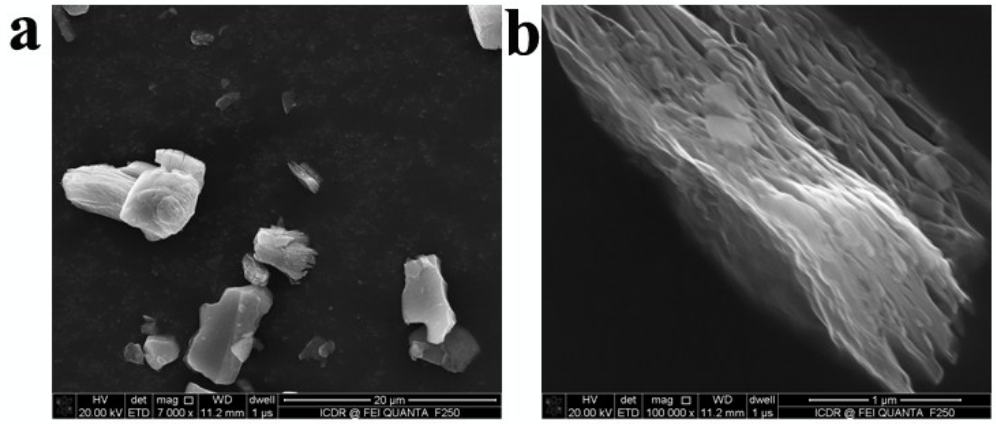

Fig. S2. SEM images of the N-$Ti_3C_2T_x$-500 sample (a, b).

Fig. S3

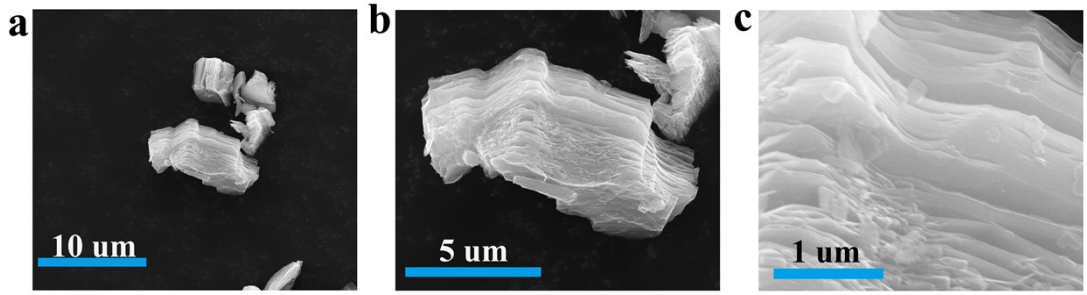

Fig. S3 SEM images of the N-$Ti_3C_2T_x$-200 sample (a, b and c).

Fig. S4

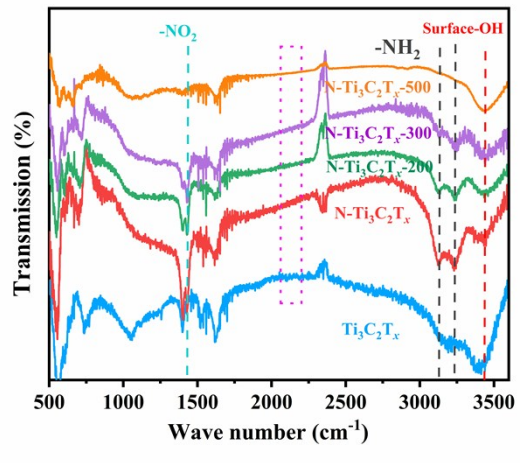

Fig. S4 FTIR transmission spectra of the $Ti_3C_2T_x$, N-$Ti_3C_2T_x$, N-$Ti_3C_2T_x$-200, N-$Ti_3C_2T_x$-300 and N-$Ti_3C_2T_x$-500 samples.

The $-NH_2$ was characterized by the peak at 3158 and 3265 cm^{-1}, The surface -OH was characterized by the peak at 3370 cm^{-1}, and The $-NO_2$ was characterized by the peak at 1420 cm^{-1}. The peak at the 812 and 1535 cm^{-1} peak didn't detected due to the disturbance of noise in this mode.

Fig.S5

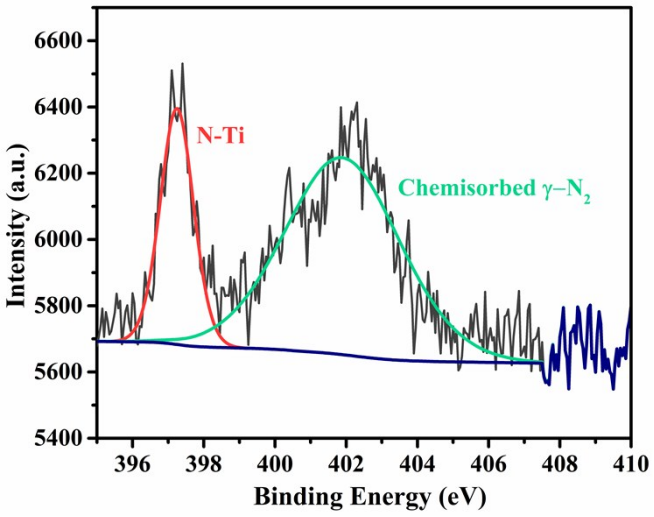

Fig. S5 XPS spectra of the deconvoluted N 1s peaks of the $Ti_3C_2T_x$ sample.

Fig. S6

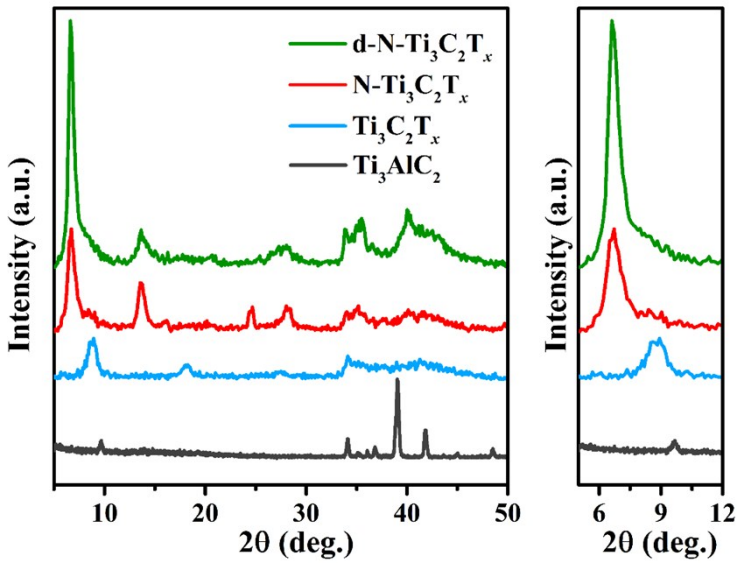

Fig. S6 XRD patterns of the d-N-$Ti_3C_2T_x$, N-$Ti_3C_2T_x$, $Ti_3C_2T_x$ and Ti_3AlC_2 samples and magnified patterns over 5-12°.

Fig. S7

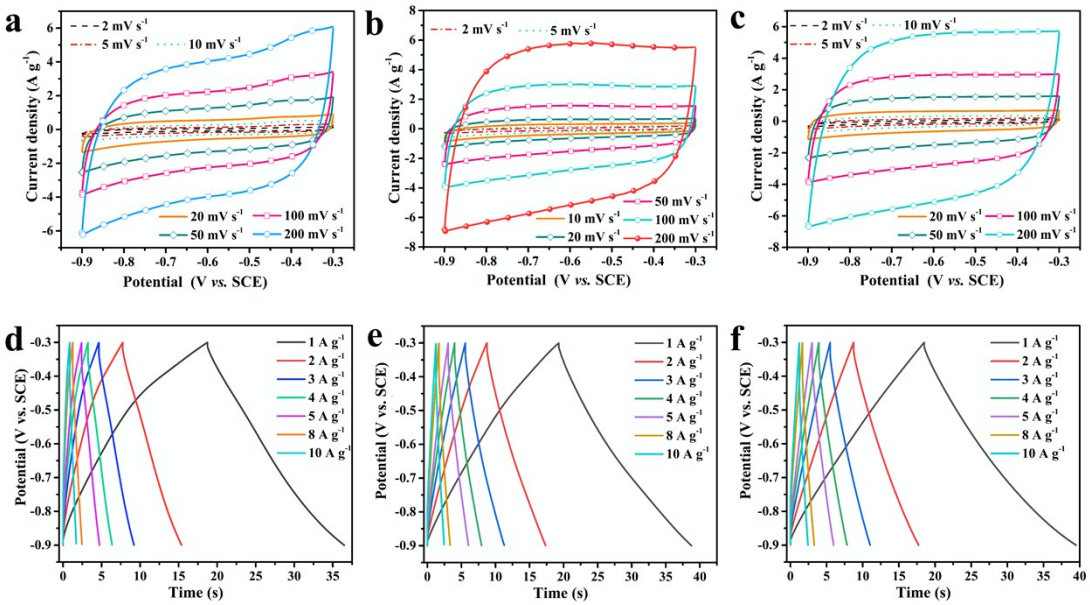

Fig. S7 (a) CV curves of the $Ti_3C_2T_x$ based electrode at scan rates from 2 mV s^{-1} to 200 mV s^{-1}, in 1 M Li_2SO_4. (b) CV curves of the N-$Ti_3C_2T_x$ based electrode at scan rates from 2 mV s^{-1} to 200 mV s^{-1}. (c) CV curves of the N-$Ti_3C_2T_x$-500 based electrode at scan rates from 2 mV s^{-1} to 200 mV s^{-1}. (d) GCD curves of the $Ti_3C_2T_x$ based electrode at current densities from 1 A g^{-1} to 10 A g^{-1}. (e) GCD curves of the N-$Ti_3C_2T_x$ based electrode at current densities from 1 A g^{-1} to 10 A g^{-1}. (f) GCD curves of the N-$Ti_3C_2T_x$-500 based electrode at current densities from 1 A g^{-1} to 10 A g^{-1}.

Fig. S8

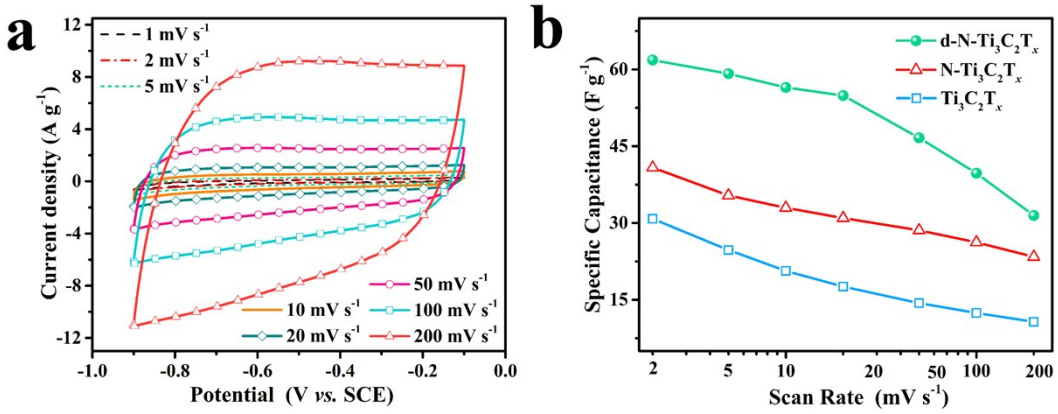

Fig. S8 (a) CV curves of the d-N-$Ti_3C_2T_x$ based electrode at scan rates from 2 mV s^{-1} to 200 mV s^{-1}, in 1 M Li_2SO_4. (b) Specific capacitances of the $Ti_3C_2T_x$, N-$Ti_3C_2T_x$ and d-N-$Ti_3C_2T_x$ electrodes at different scan rates.

The above results confirm that the NH_4F/HCl mixture is an effective etchant to exfoliate $Ti_3C_2T_x$, as evidenced by the TEM images shown in Fig.S3. The exfoliated $Ti_3C_2T_x$ (d-N-$Ti_3C_2T_x$) has a capacitance of as high as 62 F g^{-1} at 2 mV s^{-1}, probably because more active sites are introduced during the exfoliation progress.

Fig. S9

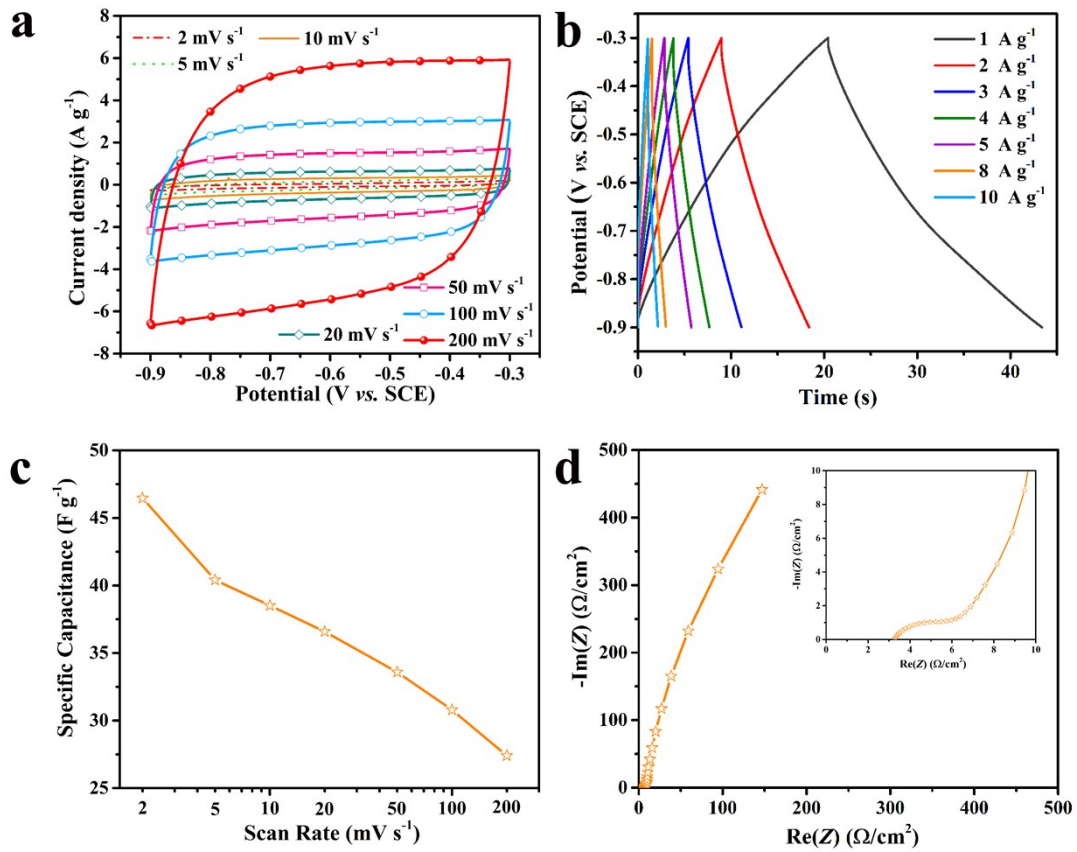

Fig. S9 (a) CV curves of the N-$Ti_3C_2T_x$-200 based electrode at scan rates from 2 mV s^{-1} to 200 mV s^{-1}, in 1 M Li_2SO_4. (b) GCD curves of the N-$Ti_3C_2T_x$-200 based electrode at current densities from 1 A g^{-1} to 10 A g^{-1}. (c) Specific capacitance of the N-$Ti_3C_2T_x$-200 electrode at different scan rates. (d) Nyquist plot of the N-$Ti_3C_2T_x$-200 electrode from 100 kHz to 10 mHz. The inset is a magnification in the high-frequency region.

Fig. S10

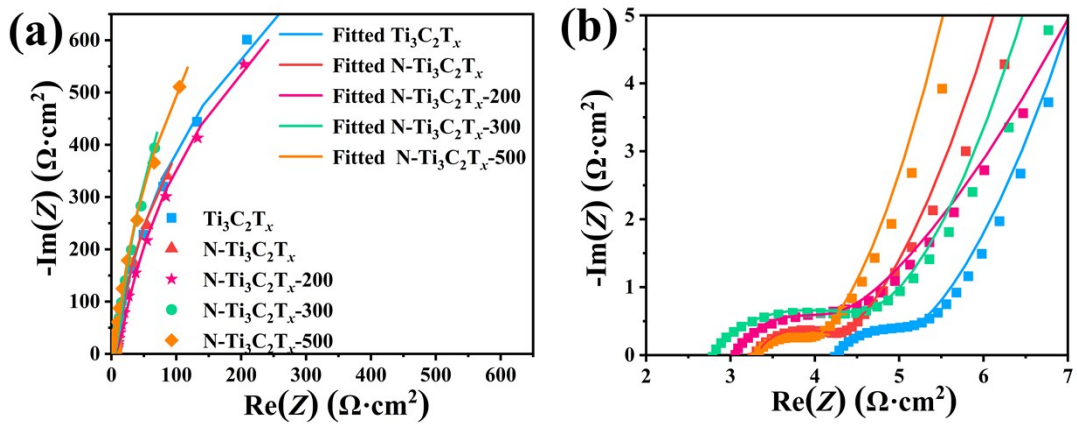

Fig.S10 The fitted curves for the $Ti_3C_2T_x$, N-$Ti_3C_2T_x$, N-$Ti_3C_2T_x$-200, N-$Ti_3C_2T_x$-300 and N-$Ti_3C_2T_x$-500 samples.

Fig. S11

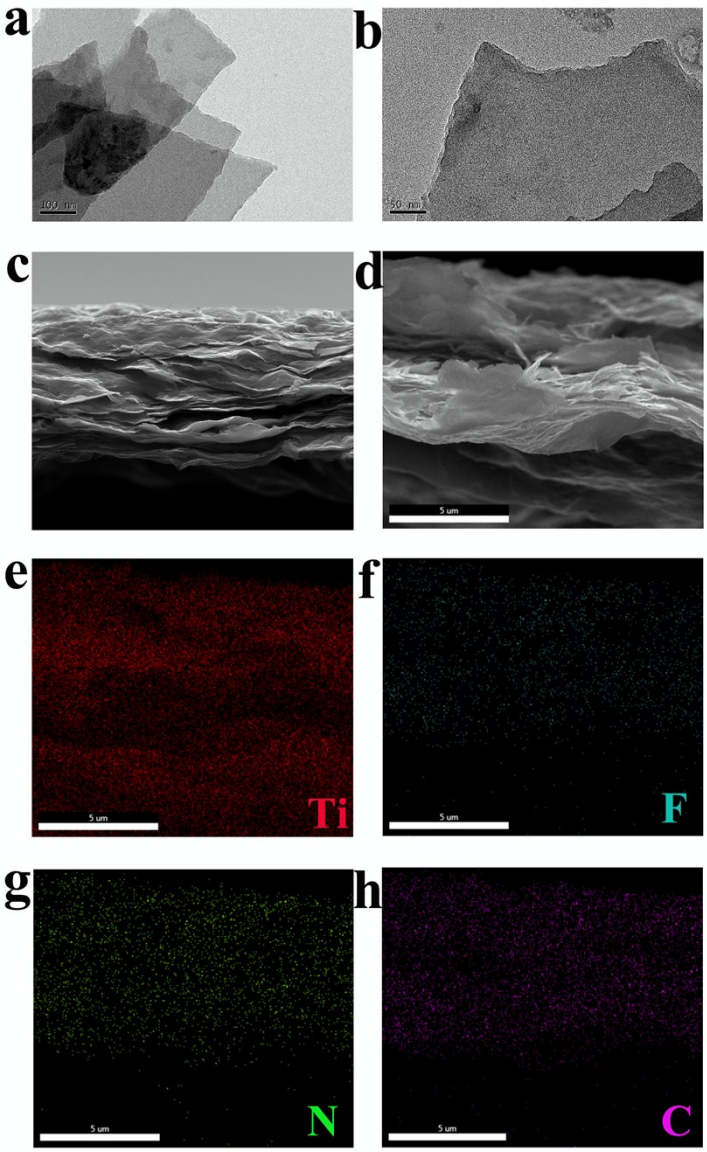

Fig. S11 (a-b) TEM images of the $Ti_3C_2T_x$ nanosheets, (c) Cross section SEM images of the N-$Ti_3C_2T_x$-300 films, (d-h) SEM images of the N-$Ti_3C_2T_x$-300 films, (e, f, g and h) EDS elemental mappings of Ti, F, N and C.

The TEM images of the $Ti_3C_2T_x$ nanosheets are shown in the Fig. S10 a-b, which indicate the $Ti_3C_2T_x$ are ultrathin nanosheets. Figs. S10 c-d show the cross section images of the N-$Ti_3C_2T_x$-300 films. Furthermore, the Figs. S10 e-h show the Elemental distribution profiles of C, N, F and Ti of the N-$Ti_3C_2T_x$-300 film, indicating that the elements are uniformly distributed within the N-$Ti_3C_2T_x$-300 film.

Fig. S12

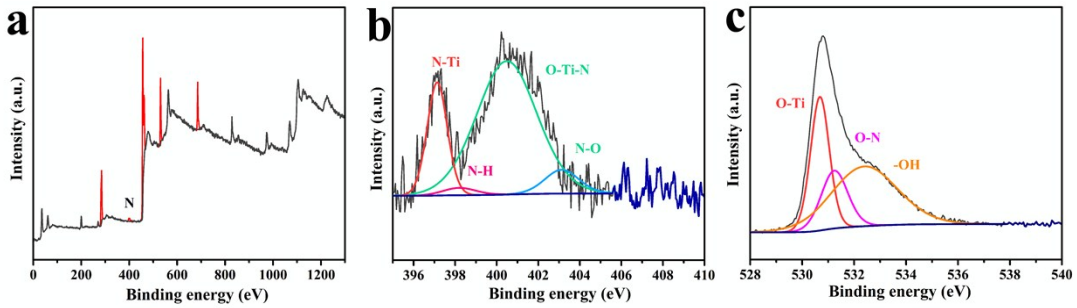

Fig. S12 (a) XPS survey spectrum of the N-$Ti_3C_2T_x$-300 films. (b) High-resolution XPS spectra of the deconvoluted N 1s peaks of the N-$Ti_3C_2T_x$-300 films. (c) High-resolution XPS spectra of the deconvoluted O1s peaks of the N-$Ti_3C_2T_x$-300 films.

Fig. S12 shows the XPS survey spectrum of the N-$Ti_3C_2T_x$-300 film and the High-resolution XPS spectra of the deconvoluted N and O1s peaks, which show a similar results with the N-$Ti_3C_2T_x$-300 powder sample. The N-Ti bond at 397.2 eV, in which the N atoms replace the C atoms in the Ti_3C_2 structure, is in accordance with the previous literature [15, 20-21]. The extra nitrogen related peaks at 398.5 eV, 400.5 eV and 403.4 eV for the N-$Ti_3C_2T_x$ sample can be assigned to -NH_2, O-Ti-N, and Ti-O-N, respectively. What's more, the O-Ti-N bond is of bigger content, which is of great importance for the electrochemical performance of SCs. Besides, the O-N bond is also observed in the O1s peaks.

Fig. S13

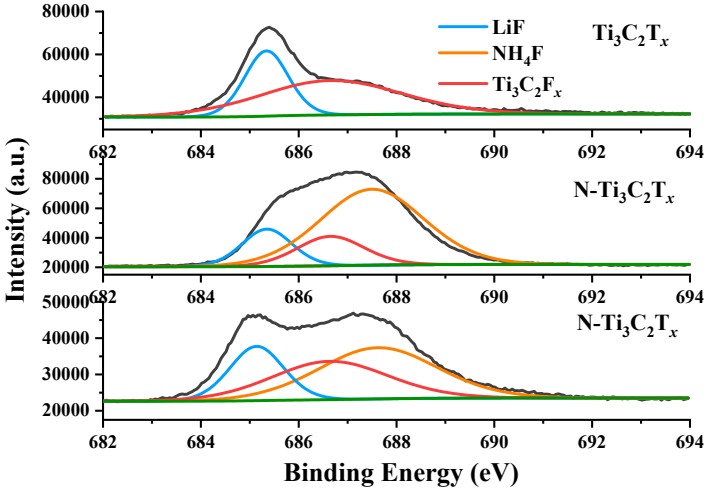

Fig. S13. F 1s XPS spectra of the $Ti_3C_2T_x$, N-$Ti_3C_2T_x$, and N-$Ti_3C_2T_x$-300 samples.

It's the Ti-F bond that influence the electrochemical performance of the MXene based SCs, not the -F in other forms. The content of the Ti-F bond in the $Ti_3C_2T_x$, N-$Ti_3C_2T_x$ and N-$Ti_3C_2T_x$-300 is in an atom ratio of 1:0.78:0.56, as shown in Fig. R1. Thus, the content of Ti-F bond shows a decrease phenomenon.

Fig. S14

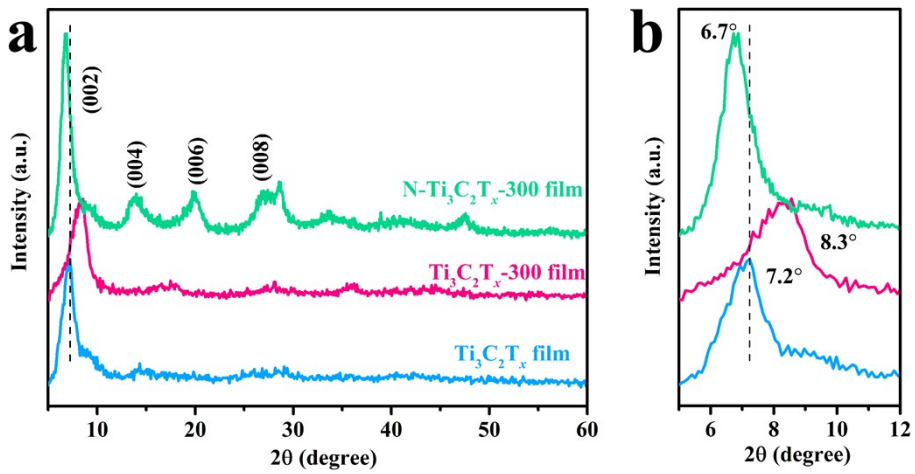

Fig.S14 The XRD spectra of the $Ti_3C_2T_x$, $Ti_3C_2T_x$-300 and N-$Ti_3C_2T_x$-300 films and the magnified patterns over 5-12°.

Fig. S14 shows the XRD spectra of the $Ti_3C_2T_x$, $Ti_3C_2T_x$-300 and N-$Ti_3C_2T_x$-300 films. It is interesting that the $Ti_3C_2T_x$-300 sample shifts to a larger degree of 8.3° compared to the $Ti_3C_2T_x$ sample, which indicates that the interlayer spacing becomes smaller due to the disappear of H_2O. That is, the N-$Ti_3C_2T_x$-300 film still shows a smaller degree of 6.7° due to the formation of the N related functional groups between the interlayer of Ti_3C_2 nanosheets.

Fig. S15

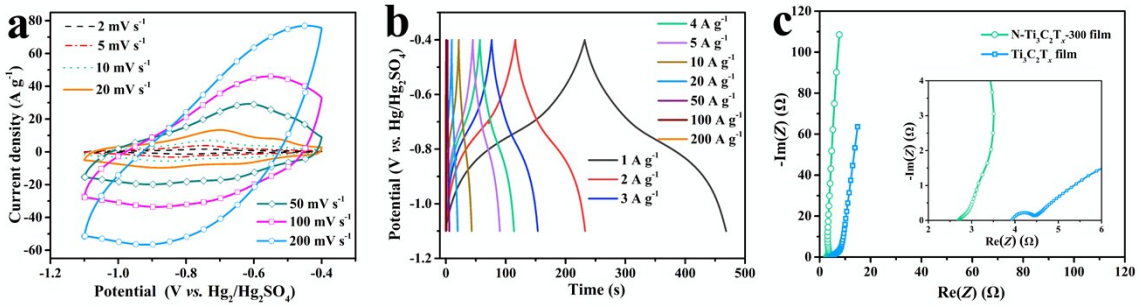

Fig. S15 (a) CV curves of the $Ti_3C_2T_x$ film electrode at scan rates from 2 mV s^{-1} to 200 mV s^{-1}, in 3 M H_2SO_4. (b) GCD curves of the $Ti_3C_2T_x$ film electrode at current densities from 1 A g^{-1} to 200 A g^{-1}. (c) Nyquist plots of the three electrodes at frequencies from 100 kHz to 10 mHz. The inset is the zoom-in profile of the high-frequency region.

Fig. S16

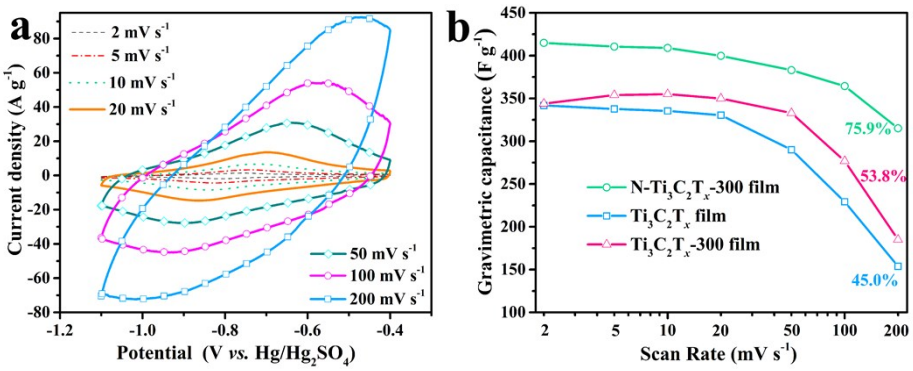

Fig. S16 Electrochemical properties tested in the three-electrode configuration with Swagelok. (a) CV curves of the $Ti_3C_2T_x$-300 film electrode at scan rates from 2 mV s^{-1} to 200 mV s^{-1}. (b) Gravimetric capacitances of the $Ti_3C_2T_x$, $Ti_3C_2T_x$-300 and N-$Ti_3C_2T_x$-300 electrodes at different scan rates.

Fig. S17

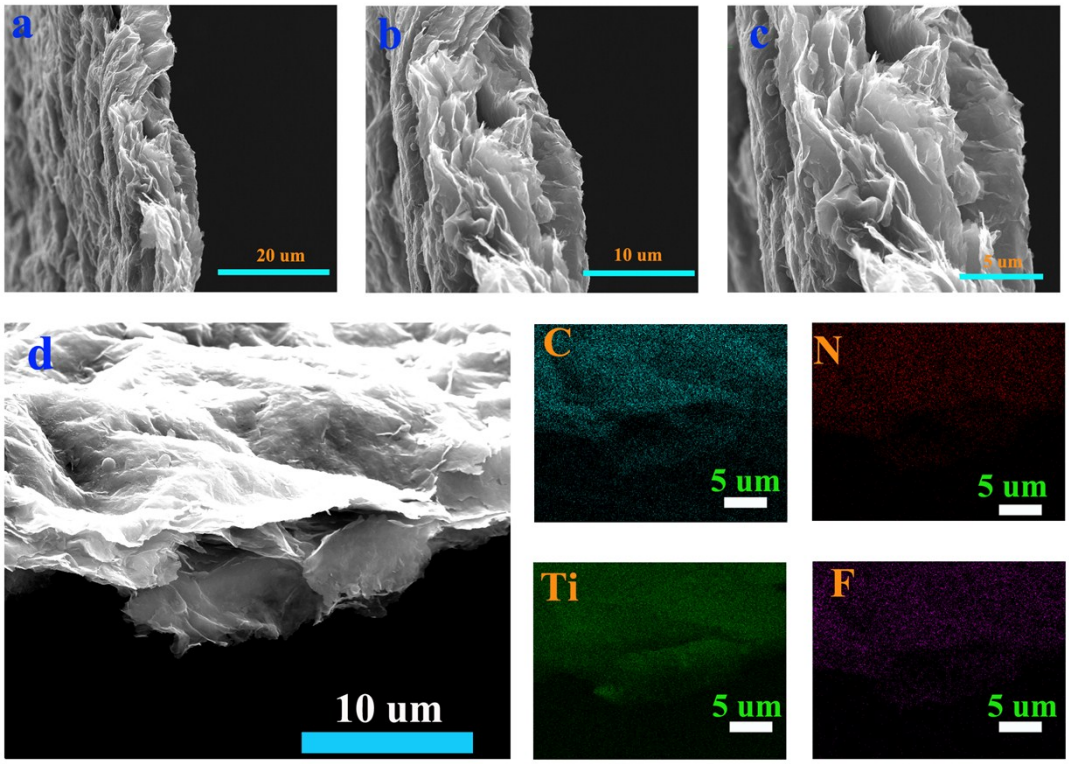

Fig. S17 SEM images of the cross section for the N-$Ti_3C_2T_x$-300 film electrode after 18000 cyclings at different magnification (a-c). (d) SEM images of the N-$Ti_3C_2T_x$-300 sample after after 18000 cyclings and the corresponding EDS elemental mappings of C, N, Ti and F.

Fig. S18

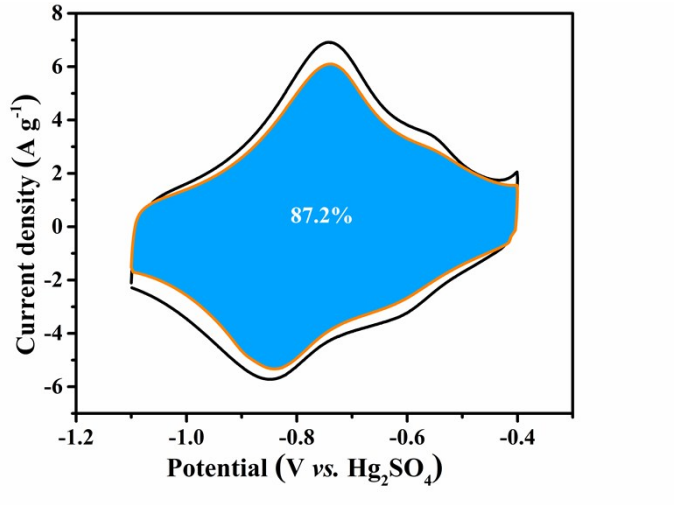

Fig. S18 CV partition analysis showing capacitive contribution to total current density at 10 mV s^{-1} for the accordion-like $Ti_3C_2T_x$ film electrode.

Fig. S19

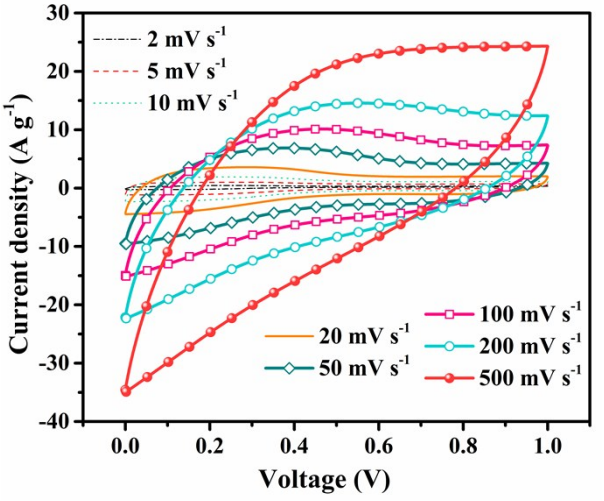

Fig. S19 CV curves of the $Ti_3C_2T_x$ film based symmetric supercapacitor at scan rates from 2 mV s^{-1} to 500 mV s^{-1} in 3 M H_2SO_4.